Assessment of Night-Time Urban Surface Temperature -- Land Use/Cover Relationship for Thermal Urban Environment Studies Using Optical and Thermal Satellite Data

Javed Mallick, India, Atiqur Rahman, India, Pham Viet Hoa, Vietnam and P.K.Joshi, India

Key words: Urban Heat Island (UHI), Impervious Surface, Surface Temperature, and Temperature Emissivity Separation (TES), Delhi

SUMMARY

Urbanization, both in geographic extent as well as in population, transforms the landscape from natural cover types to increasingly impervious urban land. The result of this change can have significant effects on local weather and climate (Landsberg, 1981). In this study, the thermal urban environment of Delhi, India is examined using satellite images provided by the ASTER sensor on board Terra satellite and LANDSAT ETM+. Two time periods (2001 and 2005) nighttime (ASTER) and daytime satellite datasets are used to analyze the spatial structure of the thermal urban environment and the 'hot' surfaces within the urban settings were identified that is related to the urban surface characteristics and land use/land cover. The method used for this study involves deriving the surface temperature using TES Temperature Emissivity Separation (TES) algorithm, constructing statistics of ASTER multi-spectral thermal infrared images and use of GIS to combine them with a land use/cover derived from satellite datasets, and with data from intensive in-situ measurements. The average images reveal spatial and temporal variations of land surface temperature (T_S) of nighttime and distinct microclimatic patterns. The combined interpretation of the images and of the land use/cover classification shows the effect of surface's physical properties.

Analysis shows that over the span of five years (2001-05), there is small increase (1-2°C) in the mean surface temperature over all land use/land cover at city level. The influence of land use/ land cover on surface temperature observed that the area having high amount of vegetation showed low mean surface temperature. A change in mean surface temperature is much higher, mainly due to the change in the land use/land cover and amount of vegetation whereas few patches of area showed decline in surface temperature. Central Business District (CBD) of Delhi, Cannaught Place, high dense built up area, commercial/industrial area displays heat islands larger than 4°C compared to the suburbs. The small increase in surface temperature at city level is mainly attributed to cumulative impact of human activates and changes in land use/ land cover pattern.

The spatial layout of the land use/ land cover in the area has a great impact on the development of urban heat islands. Therefore, urban planning should be adopted to avert or alleviate the effect of urban heat islands.

1/15

TS 1G - Remote Sensing for Sustainable Development

Javed Mallick, Atiqur Rahman, Pham Viet Hoa, and P.K.Joshi

Assessment Of Night-Time Urban Surface Temperature -- Land Use/Cover Relationship for Thermal Urban

Environment Studies Using Optical And Thermal Satellite Data

Assessment of Night-Time Urban Surface Temperature -- Land Use/Cover Relationship for Thermal Urban Environment Studies Using Optical and Thermal Satellite Data

Javed Mallick, India, Atiqur Rahman, India, Pham Viet Hoa, Vietnam and P.K.Joshi, India

INTRODUCTION

Urbanization, both in geographic extent as well as in population, transforms the landscape from natural cover types to increasingly impervious urban land. The result of this change can have significant effects on local weather and climate (Landsberg, 1981). The interactions of urban land surfaces with the atmosphere are governed by surface heat fluxes, the distribution of which is significantly modified by urbanization. The main contributing factors are changes in the physical properties of the surface (albedo, thermal capacity, heat conductivity), owing to the replacement of vegetation/natural surface by asphalt and (convert to pervious surfaces to impervious surfaces); the decrease of surface moisture available for evapotranspiration; changes in the radiative fluxes and in the near surface flow, owing to the complicated geometry of streets and tall buildings, and anthropogenic heat. This refers especially, to the distinct difference of temperature between urban and non-urbanised rural settings, called Urban Heat Island (UHI) (Stathopoulou and Cartalis, 2001).

Considerable research has performed in using remotely sensed information to detect thermal characteristics of urban surfaces. Some studies used measurements of temperature using temperature sensors mounted on car, along various routes (Yamashita, 1996). These methods are both expensive and time consuming and lead to problems in spatial interpolation. Satellite borne instruments can provide quantitative physical data at high spatial or temporal resolutions and repetitive coverage and capability of measurements of earth surface conditions (Owen et al., 1998). Voogt and Oke (2003) reviewed the use of thermal remote sensing for the study of urban climates with respect to the heat islands and describe the distinction between the atmospheric and the surface UHIs. The use of satellite infrared remote sensing in estimating the surface physical properties and variables has been investigated e.g. Carlson et al. (1981), Balling and Brazel (1988), Dousset (1989, 1991), Roth et al. (1989), Quattrochi and Ridd (1994), Owen et al. (1998), and Voogt and Oke (1998), Lo and Quattrochi, 2003; Dousset and Gourmelon, 2003). Luke Howard, a pioneer of urban climatology, first measured temperature differences across London as early as 1809 (Chandler 1968), But our understanding of urban effects on local climate is still unsatisfactory due to several difficulties: 1) the inherent complexity of the city-atmosphere system, 2) lack of a clear conceptual theoretical framework for inquiry, and 3) the high expense and enormous difficulties of acquiring a sufficient quantity of high-quality, high- resolution (both spatially and temporally) observations in cities.

The capital city of India New Delhi is expanding very fast in terms of urban sprawl. This thermal behaviour of urban surfaces over the course of a day would yield a remarkable database for urban planners and architects for improving city site quality by making it more

TS 1G - Remote Sensing for Sustainable Development

Javed Mallick, Atiqur Rahman, Pham Viet Hoa, and P.K.Joshi

Assessment Of Night-Time Urban Surface Temperature -- Land Use/Cover Relationship for Thermal Urban

7th FIG Regional Conference

Spatial Data Serving People: Land Governance and the Environment – Building the Capacity Hanoi, Vietnam, 19-22 October 2009

Environment Studies Using Optical And Thermal Satellite Data

eco-friendly. This would be particularly beneficial to country like India and some other with tropical steppe climate.

This study presents a methodology that is based on emissivity factor and correction of atmospheric effect for estimating the nighttime surface UHI intensity of urban areas using ASTER thermal images and land use/land cover database in GIS environment. The novelty of the methodology presented lies in considering spatially-averaged surface temperatures per land cover compared to point surface temperature data for inclusion in the measurement of the surface UHI intensity between the urban land covers and rural surroundings. In addition, the incorporation of land cover database in the surface UHI measurement makes the method applicable to all Indian cities and minimizes the number of assumptions considered or even the computational time needed from processing satellite data in case there is no information about the land cover distribution of a studied area (Mallick, J., 2006).

Study area:

The capital city of India, New Delhi is geographically situated between 28° 23' 17" – 28° 53' 00" North and Longitude 76° 50' 24" – 77° 20' 37" East. It lies at an altitude between 213 and 305 m and covers an area of 1,483 km². It is situated on the bank of river Yamuna. It is bordered in the east by the state of Uttar Pradesh and on the north, west, and south by the state of Haryana. The climate of Delhi is influenced by its remote inland position and prevalence of air of continental character, which is characterised by extreme summer heat in June (48 °C). alternating with severe winter cold December (3 °C). Only during the three monsoon months of July-September rainfall, oceanic air penetrates the country deep to the Northern region. The climate is of semi-arid nature due to marked diurnal differences in temperature, high saturation deficit and low/moderate annual average rainfall (60 mm). The desert area of Rajasthan to the west and south-west and the Gangetic plains of Uttar Pradesh to the east, across which the monsoon air travels and reaches Delhi, have their respective shares in affecting the climate of this region. Extreme dryness with an intense hot summer and cold winter are the features, which are associated with sweep of air from westerly or north-westerly direction, while the influx of air from the easterly or south-easterly directions usually causes increased humidity, cloudiness and precipitation. The urban population of Delhi increased at 3.87% annual growth rate during 1991-2001. The latter is influenced by the gradual shifting of the rural area and its merger with urban area. With the continuation of the present population trend, the total population of National Capital Territory (NCT) Delhi by the year 2011 and 2021 would be 18.2 million and 22.5 million respectively. As per Census 2001, NCT Delhi had a population of 13.78 million and 46.28 percent decennial population growth during 1991-2001.

SATELLITE DATA PROCESSING

ASTER

Satellite datasets of Terra ASTER level-1B (Level 1-B product contains radiometrically calibrated and geometrically co-registered data for all ASTER channels) over Delhi area of

- October 07, 2001 (Night time) of Path/row 13/204
- October 18, 2001 (Day time) of Path/row 146/40
- October 02, 2005 (Night time) of Path/row 13/204

TS 1G - Remote Sensing for Sustainable Development

3/15

Javed Mallick, Atiqur Rahman, Pham Viet Hoa, and P.K.Joshi

Assessment Of Night-Time Urban Surface Temperature -- Land Use/Cover Relationship for Thermal Urban Environment Studies Using Optical And Thermal Satellite Data

7th FIG Regional Conference

Spatial Data Serving People: Land Governance and the Environment – Building the Capacity Hanoi, Vietnam, 19-22 October 2009

have been used for preparation of land use/land cover (LU/LC) map and estimation of surface temperature. DN values were converted to at sensor radiance, for ASTER using

$$L_{\lambda} = (DN - 1) \times UCC$$

UCC is unit conversion coefficients from HDF file.

The unit conversion coefficients that are used for different bands and for different gain settings are given in ASTER User Handbook.

LANDSAT-7 ETM+

Landsat-7 ETM+ (SLC-off mode) over Delhi area of 06th and 22nd October 2005 (Day time. Level-1G product, path/row 146/40---SLC off mode) have been used in this study (cloud cover 0%). DN values were converted to at sensor radiance, for landsat-7 ETM+ using

$$L_{\lambda} = Gain \times Bias = \left(\frac{L_{\text{max}} - L_{\text{min}}}{255}\right) \times DN + Bias$$

Where,

 L_{λ} =spectral radiance at the sensor (Wm-2sr-1 μ m-1)

Biss = Lmin

ASTER level-1B and Landsat-7 ETM+ level-1G were geometrically corrected data sets. For standardization, ASTER 15 m data (VNIR) and Landsat -7 ETM+ Panchromatic data (15 m resolution) both were compared to each other and was noticed that geometrical accuracy was low. Also the GPS readings from the ground did not match with these images. Hence there was a need to further rectify the datasets. The image was geometrically rectified to a common Universal Transverse Mercator (UTM) WGS84 coordinate system and were resampled to its spatial resolution using the nearest- neighborhood algorithm.

Considering the objectives and satellite data used, following LU/LC classification scheme has been adopted: high dense built-up, low dense built-up, commercial /industrial area, dense vegetation (forest), sparse vegetation (including parks), water bodies, and fallow land, waste land/bare soil and agricultural cropland. For image classification, a pre-field visit was done to have an idea of different LU/LC classes existing in the study area. Unsupervised classification was initially performed on ASTER and Landsat-7 ETM+ for an idea of the spectral separability of the land use/land cover classes. An extensive field survey was done with the priori knowledge using the unsupervised classification to identify sample points in the imagery for different LU/LC classes at various locations using GPS. Based on the collected sample sets for respective LU/LC classes, training sets were selected in the False Color Composite (FCC) imagery for supervised classification using Maximum Likelihood Classification (MLC). Minimum Noise Fraction (MNF) was performed on the ASTER and Landsat-7 ETM+ data to reduce the data redundancy and correlation between spectral bands. MNF was applied to bands 1 to 7 (excluding band 6) on Landsat-7 ETM+ dataset and band 1 to 3 on ASTER. The first three MNF components of Landsat-7 ETM+ and Aster data was used to classify the image using the MLC while the other components were discarded due to the higher proportion of noise content.

As mentioned, Landsat 7 ETM+ datasets (SLC-off mode) have been used for landuse/cover classification. Due to the SLC failure, Landsat-7 ETM+ data were captured of 22% of missing scene area. So to fill up these gaps a selected pairs were acquired from two -16-day coverage

TS 1G - Remote Sensing for Sustainable Development

4/15

Javed Mallick, Atiqur Rahman, Pham Viet Hoa, and P.K.Joshi

Assessment Of Night-Time Urban Surface Temperature -- Land Use/Cover Relationship for Thermal Urban Environment Studies Using Optical And Thermal Satellite Data

cycles. Both images were processed separately (upto landuse/cover classification). Later a model has been created in ERDAS (Spatial Model Maker) ---using EITHER IF statement to fill the gaps.

EITHER first image IF (first image >0) OR second image OTHERWISE

It is presumed that the land use/land cover which was classified from 06th and 22nd October 2005 of LANDSAT 7 ETM+ have not been changed during this period.

METHODOLOGY

Temperature Emissivity Speparation (TES) algorithm

Gillespie et al. (1998) proposed a new Temperature Emissivity Separation (TES) technique for Terra ASTER data. TES attempts to compensate for reflected down welling irradiance and estimates the absolute spectral emissivity. The additional constraint to overcome the under-determination comes from the regression of the minimum emissivity of spectral contrast (calculated from laboratory spectra), used to equalize the number of unknowns and measurements, so that the set of Planck's equations for the measured thermal radiances can be inverted. ASTER has 14 spectral bands, out of which 5 thermal bands (10-14) operate between 8-12 µm. In this study, five emissivity and one surface temperature maps were produced using the TES algorithm. It not only estimates the temperature of homogeneous areas of known emissivity, such as water bodies, but also for heterogeneous areas of unknown emissivity. The spectral radiance of thermal bands at the sensor is calculated using equation 2.

$$LS_{j} = \left[\varepsilon_{j} L^{BB}_{j}(T) + \left(1 - \varepsilon_{j}\right) L_{j}^{sky}\right] \times \tau_{j} + L_{j}^{atm}$$
(2)

Where,

 LS_i = spectral radiance observed by the sensor,

 ε_j = surface emissivity at wavelength j,

 $L^{BB}_{j}(T)$ = spectral radiance from a blackbody at surface temperature T,

 L_j^{sky} = spectral radiance incident upon the surface from the atmosphere (downwelling), from MODTRAN,

 L_j^{atm} = spectral radiance emitted by the atmosphere (upwelling), from MODTRAN

 τ_i = spectral atmospheric transmission, from MODTRAN.

The at-sensor radiance data were corrected for atmospheric effects to obtain the radiance emitted by the surface (L_j) , using the MODTRAN radiative transfer model. The standard atmospheric parameter (tropical climate) has been considered. The retrieved output parameters were used to estimate the radiance using equation 3 & 4.

$$L_{j} = \left[LS_{j} - L_{j}^{atm} \div \tau_{j} \right] - \left(1 - \varepsilon_{j} \right) L_{j}^{sky} = \varepsilon_{j} L^{BB}_{j} (T)$$
(3)

TS 1G - Remote Sensing for Sustainable Development

Javed Mallick, Atiqur Rahman, Pham Viet Hoa, and P.K.Joshi

Assessment Of Night-Time Urban Surface Temperature -- Land Use/Cover Relationship for Thermal Urban Environment Studies Using Optical And Thermal Satellite Data

7th FIG Regional Conference

Spatial Data Serving People: Land Governance and the Environment – Building the Capacity Hanoi, Vietnam, 19-22 October 2009

Where,
$$L^{BB_j}(T) = \frac{C_1}{\lambda_j^5 \left[\exp(C_2 / \lambda_j T) - 1 \right]}$$

Hence,

$$L_{j} = \varepsilon_{j} \times \frac{C_{1}}{\lambda_{i}^{5} \left[\exp\left(C_{2}/\lambda_{i}T\right) - 1 \right]}$$

$$\tag{4}$$

Where,

 C_1 = First radiation constant = 3.74151×10⁻¹⁶

 C_2 = First radiation constant = 0.0143879 (mk)

 λ_i = Wavelength of channel j, (m)

T =Temperature

In the above equation, if the surface emissivity is known, it is possible to correct for the reflected sky radiation. The surface temperature then can be calculated using equation 5.

$$T_{j} = \frac{C_{2}}{2 \ln \left[\left(\varepsilon_{j} C_{1} / L_{\lambda} \lambda^{5} \pi \right) + 1 \right]}$$

$$(5)$$

The above equation shows that for radiance measured in 'n' spectral channels, there will be 'n+1' unknowns, 'n' emissivities and one surface temperature. In TES (Gillespie et al., 1998; Schmugge et al., 1998) the estimated kinetic temperature T is taken to be the maximum temperature, estimated from the radiance for the five ASTER TIR spectral bands, computed from equation 5, and using an assumed emissivity value (typically 0.97) in order to be within ± 0.03 for typical land surfaces (heterogeneous lands). The relative emissivities ' β_j ' were computed by the following equations:

$$\beta_{j} = \left(L_{j} / \overline{L_{j}}\right) \times \left(\overline{L^{BB}} / L^{BB} \left(\lambda_{j}, T\right)\right) \tag{6}$$

Where,

$$\overline{L_j} = (1/5) \sum_{j=1}^{j=5} L_j , \qquad (7)$$

$$L^{BB}_{j}(T) = \frac{C_{1}}{\lambda_{j}^{5} \left[\exp\left(C_{2}/\lambda_{j}T\right) - 1 \right]}$$
(8)

$$\overline{L^{BB}(T)} = (1/5) \sum_{j=1}^{j=5} L_j^{BB}(T)$$
(9)

For emissivities between 0.7 – 1.0, the ratios β_i are generally within 0.7 – 1.4.

TS 1G - Remote Sensing for Sustainable Development

6/15

Javed Mallick, Atiqur Rahman, Pham Viet Hoa, and P.K.Joshi

Assessment Of Night-Time Urban Surface Temperature -- Land Use/Cover Relationship for Thermal Urban Environment Studies Using Optical And Thermal Satellite Data

The maximum-minimum difference between the emissivity ratios β_j is given by MMD = max (β_j) - min (β_j) . It was observed that MMD ranges from 0.0 to 4.0 at most (Dash et al., 2002). An empirical relation between minimum emissivity and MMD is:

$$\varepsilon_{\min} = 0.994 - 0.687 \times (MMD)^{0.737}$$
 (10)

Therefore, the revised emissivity can be computed using the beta (β_j) spectrum as shown below:

$$\varepsilon_{j} = \beta_{j} \left(\varepsilon_{\min} / \min(\beta_{j}) \right) \tag{11}$$

Beta (β_j) is determined from the measured surface radiance L_j (surface); new emissivity (ε_j) and surface temperature can be obtained. The resultant maps were fed into equation 2 and all the process until equation 11 where repeated so as to arrive at an acceptable emissivity measurement, which is further used. Based on the above procedures, a detailed model was developed in the ERDAS Imagine to automate the calculation of the surface Temperature and **five** Emissivity maps (as the TES algorithm generate). Figure 1 shows the methodology adopted for estimating surface temperature using TES algorithm.

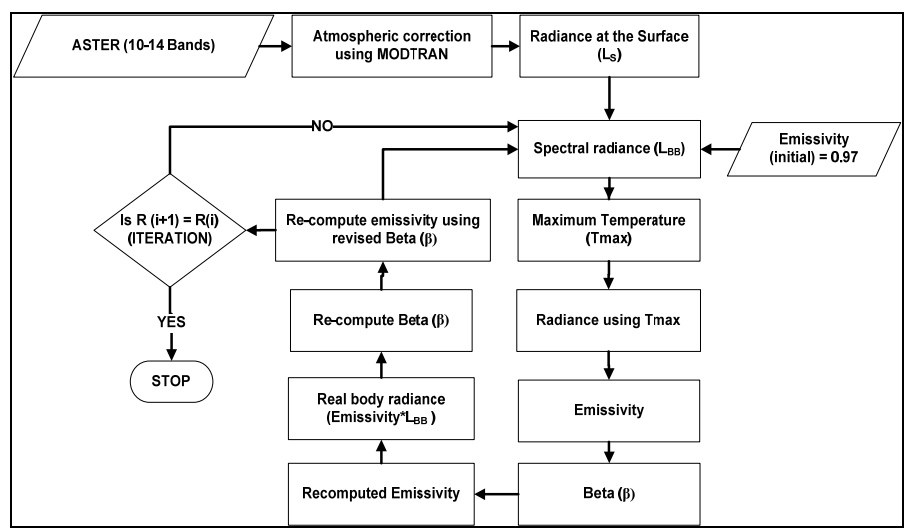


Figure1: Flow Chart for deriving surface temperature (TES) using ASTER data

RESULTS AND DISCUSSION

Analysis of Land use/Land cover

Landsat-7 ETM+ $(06^{th} and 22^{nd} Oct. 2005)$

Maximum Likelihood classification (MLC) was applied on the original bands of Landsat-7 ETM+ image. From the classified image it is observed that most of the agricultural cropland is classified as dense vegetation and sparse vegetation due to similar spectral reflectance characteristics. It is also observed that some of the sparse vegetation is getting mixed with low dense built-up and fallow land is also getting mixed with waste land/bare soil. The user's accuracy is lower in case of commercial /industrial area (55.08%), followed by sparse vegetation (66.01%) and dense vegetation (79.89%). The highest user's accuracy is found in

TS 1G - Remote Sensing for Sustainable Development

7/15

Javed Mallick, Atiqur Rahman, Pham Viet Hoa, and P.K.Joshi

Assessment Of Night-Time Urban Surface Temperature -- Land Use/Cover Relationship for Thermal Urban Environment Studies Using Optical And Thermal Satellite Data

water bodies (91.52%), followed by fallow land (86.72%) and low dense built-up (85.32%). The overall classification accuracy of 79.45% and kappa statistics of 0.7454 has been observed. It is observed that the classification results improved using the MNF components. Figure 2 shows the geographical distribution of classified land use/land cover features. The highest user's accuracy is found in water bodies (99.89%), followed by fallow land (91.12%), agricultural cropland (90.82%), low dense built-up (89.24%), dense vegetation (82.68%) and sparse vegetation (73.20%). Lower user's accuracy is found over commercial/industrial areas (62.32%). Analyzing the classification results, improvement in user's accuracy is observed over water bodies (8.37% higher) followed by commercial /industrial area (7.24%) and sparse vegetation (7.19% higher) compared to classification (MLC) using original bands. Less improvement in user's accuracy is found in high dense built-up area (2.49% higher) and waste land/bare soil (3.01%) compared to conventional classification of original bands using MLC.

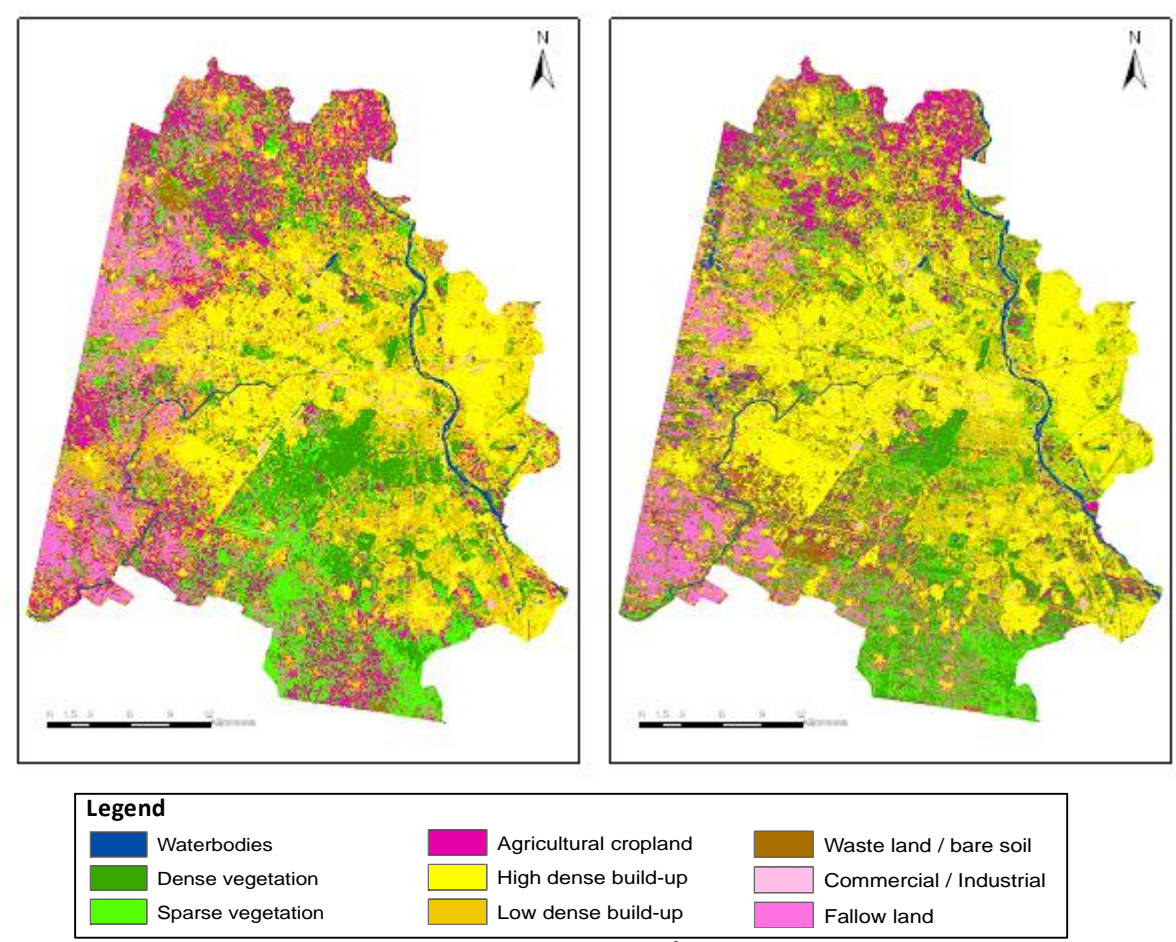


Figure2: Land use/land cover of Delhi using ASTER (18thOct.2001) and Landsat7ETM+ (Oct.2005)

An overall improved classification accuracy of 84.59% and kappa statistics of 0.8101 is observed. The classified image with original bands showed low accuracy due to the fact that there are regions of spectral overlapping of features. It is observed that Maximum Likelihood classification with MNF components significantly increases the user's accuracy over water bodies, sparse vegetation, dense vegetation, and agricultural cropland. This is mainly attributed to the reduction in noise and decrease in spectral correlation between bands.

TS 1G - Remote Sensing for Sustainable Development 8/15 Javed Mallick, Atiqur Rahman, Pham Viet Hoa, and P.K.Joshi Assessment Of Night-Time Urban Surface Temperature -- Land Use/Cover Relationship for Thermal Urban Environment Studies Using Optical And Thermal Satellite Data

ASTER (18th Oct. 2001)

The supervised classification (Maximum Likelihood classification) (MLC) was applied on the original bands as well as MNF components of ASTER image. It is observed that the classification improves using MNF components than using the MLC. After examining the error matrix, it is found that there is a good improvement in the accuracies achieved with MNF. The overall classification accuracy using MNF has been significantly improved to 86.95% and kappa statistics of 0.8509. As the uncertainties observed in land use/land cover adopted is found to be lowest with MNF, classification with MNF components for all datasets has been considered. Figure—shows the classification with MNF. It is observed that classification has been improved and thus the land use/land cover features are distinguished. The higher accuracy is found in water bodies (99.94), followed by fallow land (97.42%), low dense build-up (93.30%) and waste land/bare soil (92.17%). Lower user's accuracy is found over dense vegetation (66.95%). It is observed that good improvement (user's accuracy) is achieved over sparse vegetation (28.5% higher), followed by fallow land (14.17% higher) and dense vegetation (11.50% higher) compared to conventional classification of actual bands using MLC. The overall classification accuracy using MNF is 86.95% and kappa statistics of 0.8509. Figure 2 shows the geographical distribution of classified land use/land cover features.

Analysis of Night-time Surface Temperature Vs LULC of ASTER, dated 07th Oct. 2001

Figure 3 shows the nighttime surface temperature of ASTER, dated 7th October 2001 (night time) at 22:35 Hrs. (local time). The estimated surface temperature ranges from 23.90 to 40.01°C (mean value of 31.40°C and standard deviation of 1.863). It is observed that in the image, central and eastern part exhibits maximum surface temperature range that corresponds to built-up areas (32 to 36°C). It is observed that some parts of north-west have lower surface temperature corresponding to wasteland/bare soil and fallow land. Water bodies exhibit maximum surface temperature during night due to high thermal capacity.

Table 1 shows the surface temperature statistics of night time data and observed over fallow land (27.44 to 31.27 °C), followed by dense vegetation (28.01 to 33.90°C), agricultural cropland (28.19 to 33.95°C) and sparse vegetation (28.21 to 33.51°C). The highest surface temperature is observed in high dense built-up areas (31.48 to 36.56°C), followed by water bodies (29.36 to 37.54°C), commercial/industrial (30.40 to 40.01°C) and low dense built-up (28.15 to 35.86°C). Fallow land and waste land/bare soil due to low thermal capacity cools down faster than other land use/land cover features. Hence fallow land, waste land/bare soil and sparse vegetation are cooler as compared to other land use/land cover features during night time.

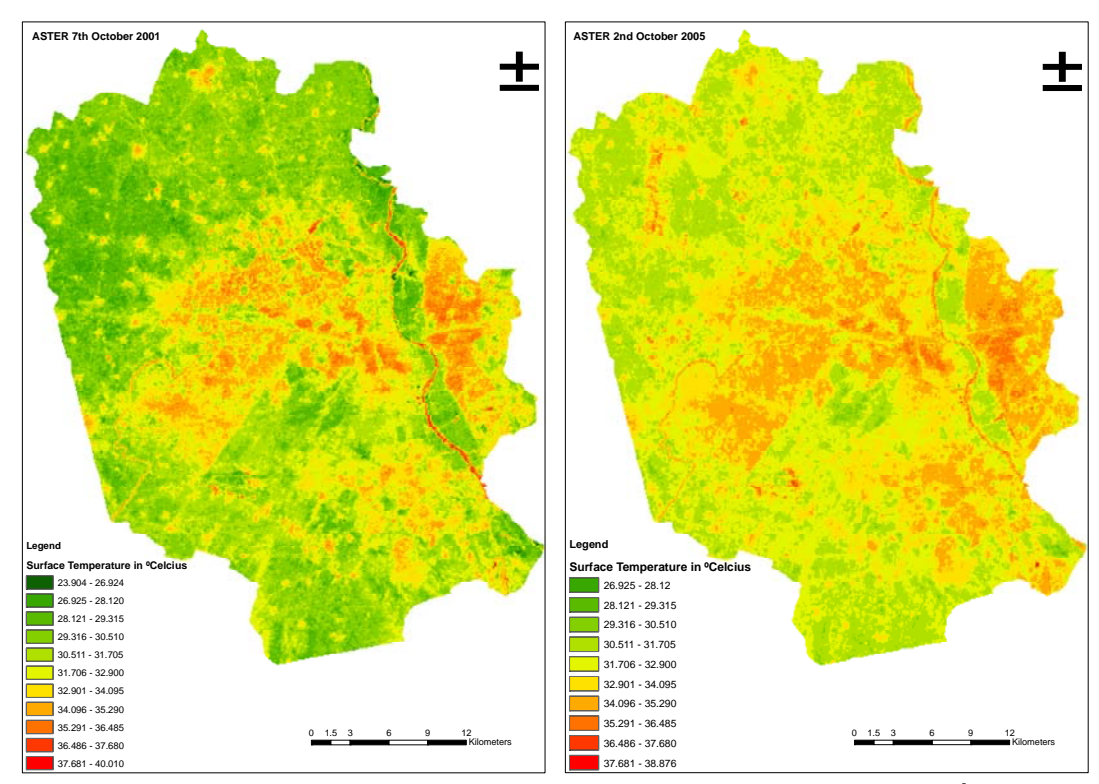


Figure 3 Spatial distribution of nighttime land surface temperature of ASTER, 7th October 2001 (night time) and 2nd October, 2005 (night time)

Table 1 Statistics of surface temperature of different LULC of ASTER (nighttime) 7th Oct. 2001

Land use / land cover	Min. temp	Max. temp	Mean (°C)	Standard Deviation (SD)
Water bodies	29.36	37.54	34.93	1.96
Agricultural cropland	28.19	33.95	29.96	0.71
Dense vegetation (forest)	28.01	33.90	29.93	1.16
Sparse vegetation	28.21	33.51	30.41	0.98
Low dense built-up	28.15	35.86	33.09	1.70
High dense built-up	31.48	36.56	35.13	0.51
Commercial/industrial	30.40	40.01	33.81	1.41
Waste land/bare soil	28.31	33.34	30.79	0.61
Fallow land	27.44	31.27	29.04	0.72

Analysis of Night-time Surface Temperature of ASTER data Vs LULC of LANDSAT7 ETM + October 2005

Figure 3 shows the night time surface temperature of ASTER, 2nd October 2005 at 22:35 Hrs. (local time). The estimated surface temperature ranges from 26.93 to 38.88°C (mean value of 32.66°C and standard deviation of 1.232). It is observed that in the image, central and eastern part exhibits high surface temperatures, corresponding to high dense built-up areas. It is observed that some parts of north-west, north-east and extreme southern part of the image have lower surface temperature corresponding to agricultural cropland, waste land/bare soil

TS 1G - Remote Sensing for Sustainable Development

Javed Mallick, Atiqur Rahman, Pham Viet Hoa, and P.K.Joshi

Assessment Of Night-Time Urban Surface Temperature -- Land Use/Cover Relationship for Thermal Urban

Environment Studies Using Optical And Thermal Satellite Data

7th FIG Regional Conference

Spatial Data Serving People: Land Governance and the Environment – Building the Capacity Hanoi, Vietnam, 19-22 October 2009

and fallow land. Surface temperature over water bodies are observed to be in the range of 33.01 to 36.00 °C during night due to high thermal capacity.

From table 2 it is seen that during night time high dense built-up shows the higher surface temperature (34.82 to 36.41°C), followed by water bodies (33.85 to 36.15°C), commercial/industrial (32.70 to 34.99°C), and low dense built-up (31.89 to 34.65°C), while fallow land, dense vegetation, agricultural cropland and sparse vegetation shows lower temperatures. It is observed that the thermal gradient during night time decreases from high dense built-up to fallow land. Fallow land, waste land/bare soil and agricultural cropland are cooler as compared to other land use/land cover features during night time due to lower thermal capacity.

Figure 4 shows the range and mean of surface temperature for different land use/land cover for ASTER night time image of 2nd October 2005. Highest surface temperature is observed over dense built-up area followed by water bodies, commercial/industrial. Low dense built-up it is found that surface temperature decrease with change of land use/land cover to non builtup. Figure 4 further shows the mean of surface temperature over different land use/land cover using two nighttime ASTER data sets

Table2 Statistics of surface temperature of different land use/ land cover of ASTER (night time) 2nd October 2005

Land use / land cover	Min. temp (°C)	Max. temp (°C)	Mean (°C)	Standard Deviation (SD)
Water bodies	33.85	36.15	35.53	0.57
Agricultural cropland	30.88	33.06	31.53	0.46
Dense vegetation (forest)	29.56	31.66	30.31	0.35
Sparse vegetation	30.11	33.50	31.95	1.01
Low dense built-up	31.89	34.65	33.66	0.56
High dense built-up	34.81	36.41	35.62	0.22
Commercial/industrial	32.70	34.99	34.11	0.46
Waste land/bare soil	30.42	32.86	32.16	0.41
Fallow land	28.85	31.28	30.32	0.45

Temporal variation of surface temperature over different land use/land cover

Figure 4 shows the night time mean surface temperature of different Land use/land cover of ASTER, dated 2nd October, 2005 and 07th October, 2001. It is observed that the profile of surface temperature over land use/land cover for both the datasets is similar. The mean surface temperature value for all land use/land cover of 2nd October 2005 is higher (0.5 to 1.6°C) to that of 7th October 2001. The differences may be due to acquisition of data in different time periods associated with conversion of pervious surfaces to impervious surfaces incorporation with some external factors too e.g. increase in the density of built up areas.

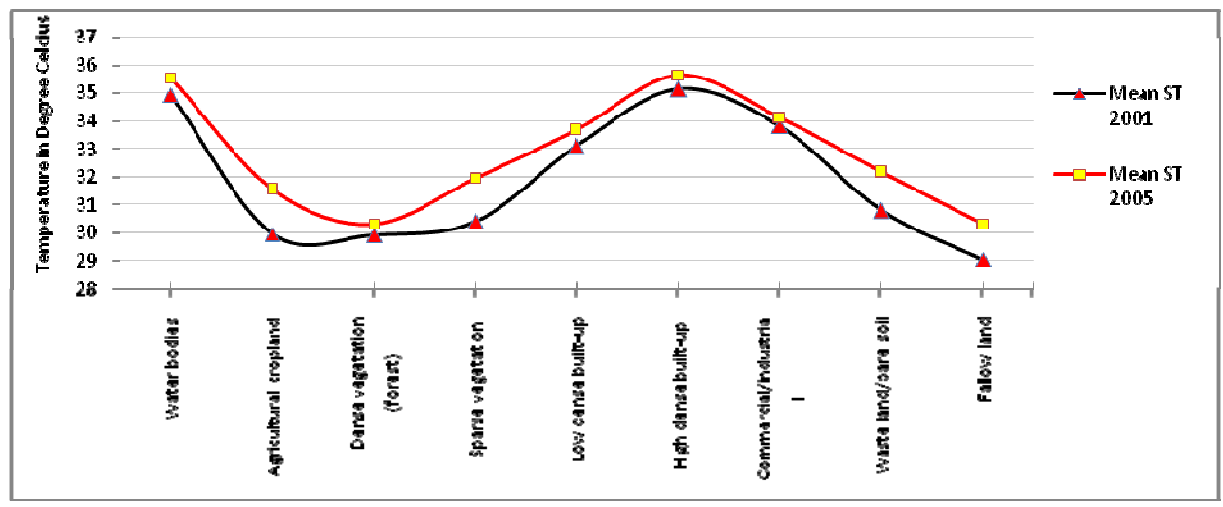


Figure 4: Night time mean surface temperature of different Land use/land cover of ASTER, dated 2nd October, 2005 and 07th October, 2001

Comparison of observed and estimated surface temperature

All the satellite datasets taken for this study is for the month of October in order to have comparative results. To compare the estimated surface temperature values from satellite data with the field measurements, a field campaign from October 3 and October 7, 2005 was carried out. All the measurement of temperature were done using TELETEMP infrared radiometer which operates in the 8-14 µm waveband with an instantaneous field of view (IFOV) of 2° with an accuracy of 0.1°C. During the campaign surface temperature measurements were taken during night for different features. In the absence of field measurement in year 2001, the estimated surface temperature values have been compared with those of the year 2005, maintaining the same period of season. In the comparison of nighttime surface temperature values from table 3, it is inferred that the field values are close to that of 2nd Oct. 2005. From the comparison between the satellite (ASTER night time, dated 2nd Oct. 2005) derived surface temperature values are in good agreement. The errors in satellite derived values are within the range of 3°C. To find out the difference between the temperatures on 2nd October and 3rd October 2005 ambient air temperature measurement were collected from Indian Meteorology department (IMD) at Sufdarjung monitoring station, Delhi. The values on 2nd Oct. 2005 were maximum 34.2°C and minimum- 23.0°C, and on 3rd Oct. 2005, maximum 34.6°C and minimum 21.5°C. Also a comparison of field measured surface temperature values with night time ASTER dated 07th October 2001 reveals that the error in estimated surface temperature is within 3°C.

Table 3 Comparison of satellite derived night time surface temperature with field measurement

	*In the field Observation on	Satellite ob		
Features	3 rd Oct 2005 (21.30 to 23.00 local time) in °C	ASTER of 7 th Oct 2001 (22.35 IST) in °C	ASTER of 2 nd Oct 2005 (22.35 IST) in °C	UTM Coordinates (m)
Vegetation 1	28.50	29.64	31.10	718935 / 3159479
Vegetation 2	29.00	30.25	31.30	719570 / 3169243
Vegetation 3	29.30	30.67	31.47	718365 / 3167032
Vegetation 4	28.00	28.95	30.20	717613 / 3160398
Average	28.70	29.88	31.02	-
Bare soil	28.50	30.88	31.35	700395 / 3158756
Concrete (URBAN-1)	28.30	35.42	32.34	717811 / 3169012
Concrete (URBAN-2)	30.10	31.90	32.96	719871 / 3168740

^{*}This measurement is the mean value 5 to 10 reading

CONCLUSION

Thermal signatures of different land use/land cover types in the study area for night time help to throw light on their roles in contributing to the urban heat island phenomenon. From the analysis, it is inferred that over the span of five years (2001-05), there is small increase (1-2°C) in the mean surface temperature over all land use/land cover at city level. The influence of land use/ land cover on surface temperature observed that the area having high amount of vegetation showed low mean surface temperature. During the five years time, changes in mean surface temperature is much higher, mainly due to the change in the land use/land cover and amount of vegetation whereas few patches of area showed decline in surface temperature. The small increase in surface temperature at city level mainly attributed due to cumulative impact of all changes in land use/ land cover and amount of vegetation in city. The spatial layout of the land use/ land cover in the area has a great impact on the development of urban heat islands. Therefore, urban planning should be adopted to avert or alleviate the effect of urban heat islands (Mc Pherson, 1994).

ACKNOWLEDGEMENTS

The authors acknowledge their sincere gratitude to Vice-Chancellor, and Head of Department, Jamia Millia Islamia University for the support, constant encouragement and useful suggestions during the course of this research work.

REFERENCES

- 1. Aniello, C., K. Morgan, A. Busbey, and L. Newland, 1995: Mapping micro-urban heat islands using Landsat TM and a GIS. Computers and Geosciences 21(8), 965-967.
- 2. Balling, R.C., and S.W. Brazel, 1988: High- resolution surface temperature patterns in a complex urban terrain. Photogrammetric Engineering and Remote Sensing 54(9), 1289-1293.
- 3. Carlson, T.N., J.K. Dodd, S.G. Benjamin, and J.N. Cooper, 1981: Satellite estimation of the surface-energy balance, moisture availability and thermal inertia. Journal of Applied Meteorology 20(1), 67-87.
- 4. Chandler, T.J., 1968: Urban climates. Proceedings of the Symposium on Urban Climates and Building Climatology, Brussels, October 1968, World Meteorological Organization, Technical Note 1(108).
- 5. Dash P., Gottsche, F.M., Olesen, F.S., and Fischer, H., 2002, Land surface temperature and emissivity estimation from passive sensor data: theory and practice-current trends: International Journal of Remote Sensing, v.23 (13), p.2563-2594.
- 6. Dousset, B., 1989: AVHRR-derived cloudiness and surface temperature patterns over the Los Angeles area and their relationships to land-use. *Proc. IGARSS-89*, Vancouver, BC, Canada, IEEE, 2132–2137.
- 7. Dousset, B., "Surface temperature statistics over Los Angeles: the influence of land use," in Proceedings of IGARSS-91, pp. 367-371, I.E.E.E., 1991.
- 8. Dousset B. and F. Gourmelon, 2003: Satellite multi-sensor data analysis of urban surface temperatures and landcover. ISPRS Journal of Photogrammetry and Remote Sensing 58(1-2), 43-54.
- 9. Gillespie, A., Shuichi Rokugawa, Tsuneo Matsunaga, J. Steven Cothern, Simon Hook, and Anne B. Kahle, 1998, A temperature and emissivity separation algorithm for Advanced Space borne Thermal Emission and Reflection Radiometer (ASTER) images: IEEE Transactions on Geosciences and Remote Sensing, v.36(4), p. 1113-1126.
- 10. Mallick, J., 2006, Satellite-based analysis of the role of land use land cover and vegetation density on surface temperature regime of Delhi, India. Enschede, ITC, The Netherlands.
- 11. Landsberg, H.E., 1981, the urban climate, New York: Academic Press.
- 12. Lo, C.P. and D.A. Quattrochi, 2003: Land- use and land-cover change, urban heat island phenomenon, and health implications: A remote sensing approach. Photogrammetric Engineering and Remote Sensing 69(9), 1053-1063.
- 13. Kaufmann, Y.J., Wald, A.E., Remer, L.A., Gao, B.C., Li, R.R., and Flynn, L., The MODIS 2. μm Channel-Correlation with visible reflectance for use in remote sensing of aerosol: IEEE Transactions on Geo-science and Remote Sensing, v. 35, p.1286-1298.
- 14. Owen, T.W., Carlson, T.N., Gillies, R.R., 1998, Remotely sensed surface parameters governing urban climate change: Internal Journal of Remote Sensing. v.19, p.1663–1681.

- 15. Quattrochi, D.A. and M.K. Ridd, 1994: Measurement and Analysis of thermal energy responses from discrete urban surfaces using remote sensing data. International Journal of Remote Sensing 15(10), 1991-2022.
- 16. Roth, M., Oke, T. R., and Emery, W. J., 1989, Satellite-derived urban heat islands from three coastal cities and the utilization of such data in urban climatology: International Journal of Remote Sensing, v.10, p.1699-1720.
- 17. Schmugge, T., Hook, S.J., and Coll, C., 1998, Recovering Surface Temperature and Emissivity from Thermal Infrared Multi spectral Data. Remote Sensing of Environment, v. 65: p.121-131.
- 18. Stathopoulou, M. and Cartalis, C., 2001, Daytime urban heat islands from Landsat ETM+ and Corine land cover data: An application to major cities in Greece. Solar Energy 81 358–368
- 19. Streutker D.R., 2002: A remote sensing study of the urban heat island of Houston, Texas. International Journal of Remote Sensing 23(13), 2595-2608.
- 20. Voogt, J.A. and T.R. Oke, 1998: "Effects of urban surface geometry on remotely-sensed surface temperature", International Journal of Remote Sensing, 19, 895-920.
- 21. Voogt, J.A., Oke, T.R., 2003. Thermal remote sensing of urban climates. Remote Sensing of Environment 86 (3): 370–384.
- 22. Yamashita, 1996, Detail Structure of Heat Island Phenomena from Moving Observations from Electric Trans Cars in Metropolitan Tokyo: Atmospheric Environment, v. 30, p.429 435.

CONTACTS

Javed Mallick *, Atiqur Rahman a*, Pham Viet Hoa b* and P.K.Joshi c*

- * Research Fellow, ^a* Sr. Assistant Professor Jamia Millia Islamia, New Delhi, India,
- b* Technology Remote Sensing, GIS and GPS, Space Technology Institute, VAST, Vietnam

Corresponding author: javnaffi@gmail.com

Javed Mallick Research Fellow

Department of Geography, Faculty of Natural Sciences Jamia Millia Islamia, Jamia Nagar, New Delhi, India

Pho: 91-11-26981717-- Ext. 3312

Fax: 91-11-26980229

^c*Associate Professor TERI University, New Delhi, India